Resonant Collision Broadening of the $(6s^2 6p7s)^3P_1^\circ$ State in Lead*

W. HAPPER AND E. B. SALOMAN†
Columbia Radiation Laboratory, Columbia University, New York, New York
(Received 13 February 1967)

Orientation and alignment depolarization cross sections have been measured for the $(6s^2 6p7s)^3P_1^\circ$ excited state of lead. The cross sections are characteristic of resonance collision broadening; $\sigma_{a1}=7.6\times10^{-13}$ cm^2 for $v_{rel}=5\times10^4$ cm/sec. The ratio of orientation broadening to alignment broadening was found to be $\gamma_1/\gamma_2=1.21(5)$. Expressions are derived for the signal shapes in Hanle-effect, optical-double-resonance, and light-beat experiments that show which components of the signals depend on orientation and alignment relaxation times, respectively.

I. INTRODUCTION

FOR sufficiently rarefied atomic vapors, the idealized picture of a free atom interacting with the radiation field provides an accurate model for the interpretation of optical-double-resonance[1] and related experiments.[2] At higher densities, however, it is necessary to consider the effects of the atoms upon each other. The interaction between an excited atom and an identical ground-state atom is particularly interesting since the long-range part of this interaction can be calculated exactly in terms of simple physical parameters. Consider an excited atom A with a dipole moment operator $\mathbf{P}_A$ located at a distance $\mathbf{R}$ from an identical (ground-state) atom B with a dipole moment operator $\mathbf{P}_B$. The light emitted by the excited atom when it falls to the ground state has a wavelength $\lambda=2\pi/k$. Then the effective interaction Hamiltonian at large distance is[3,4]

$$\mathcal{H}=-k_0^3 e^{ik_0R}\left\{(k_0R)^{-1}\left[\mathbf{P}_A-\frac{(\mathbf{P}_A\cdot\mathbf{R})\mathbf{R}}{R^2}\right]\exp(ik_0v_{||}t)\right.$$
$$\left.+\left[\frac{1}{(k_0R)^3}-\frac{i}{(k_0R)^2}\right]\left[\frac{3(\mathbf{P}_A\cdot\mathbf{R})\mathbf{R}}{R^2}-\mathbf{P}_A\right]\right\}\cdot\mathbf{P}_B. \quad (1)$$

This expression has a simple classical interpretation. It is just the interaction of two Hertzian oscillators coupled by their electric fields.[5] At very large distances only the first term (the "radiation" field) causes a significant coupling of the atoms. This long-range interaction is responsible for the phenomena associated with radiation trapping; for instance, the coherence narrowing of optical-double-resonance linewidths arises from this term.[4] When a pair of identical atoms is on the order of an optical wavelength apart, they begin to interact predominantly via the "near" fields, represented by the terms in $1/R^2$ and $1/R^3$ of Eq. (1). This short-range interaction is responsible for the "resonance" collision broadening of optical-double-resonance linewidths.[6] Such broadening results from close binary encounters between an excited atom and an identical ground-state atom. During such encounters the optical excitation can be transferred from one atom to the other in a manner analogous to spin exchange between paramagnetic atoms.[7]

Although extensive theoretical work on resonant collision broadening exists in the literature,[6,8,9] there seem to be no reliable experimental data. Careful experimental measurements of the self-broadening of cadmium double-resonance linewidths have been made.[10] However, the oscillator strength of the resonance line involved is so small ($f=0.002$) that higher-order processes dominate during a collision so that the self-broadening is essentially nonresonant and is similar to foreign-gas broadening.[6] In this work we report on the results of experimental studies of the self-broadening of the Hanle-effect linewidth in the first $^3P_1^\circ$ state of lead. The absorption oscillator strength to this level is large enough ($f=0.17$)[11] to ensure that resonant collision broadening should predominate.

The magnetic fields involved in optical-double-resonance experiments are normally too small to prompt one to speak of transverse and longitudinal relaxation times. The excited atoms are subject to an essentially isotropic environment. Consequently, if the atom has no nuclear spin, each multipole moment of the excited atom should decay with a characteristic relaxation time. In optical-double-resonance experiments, the signal linewidths reflect the relaxation rates of two atomic multipole moments, the ensemble averaged magnetic dipole moment of the excited state and the ensemble averaged electric quadrupole moment of the excited state. An ensemble of atoms with a nonzero

* Work supported by the Joint Services Electronics Program (U.S. Army, U.S. Navy, and U.S. Air Force) under Contract No. DA-28-043 AMC-00099(E).
† Present address: Department of Physics, Brown University, Providence, Rhode Island.
[1] J. Brossel and F. Bitter, Phys. Rev. **86**, 308 (1952).
[2] W. Hanle, Z. Physik **30**, 93 (1924).
[3] M. J. Stephen, J. Chem. Phys. **40**, 669 (1964).
[4] J. P. Barrat, J. Phys. Radium **20**, 541 (1959); **20**, 633 (1959).
[5] See any elementary textbook on electromagnetic theory, for instance, W. K. H. Panofsky and M. Phillips, *Classical Electricity and Magnetism* (Addison-Wesley Publishing Company, Inc., Reading, Massachusetts, 1956), p. 220.
[6] F. W. Byron, Jr., and H. M. Foley, Phys. Rev. **134**, A625 (1964).
[7] E. M. Purcell and G. B. Field, Astrophys. J. **124**, 542 (1956).
[8] A. Omont, J. Phys. Radium **26**, 26 (1965).
[9] M. I. D'yakonov and V. I. Perel', Zh. Eksperim. i Teor. Fiz. **48**, 345 (1965) [English transl.: Soviet Phys.—JETP **21**, 227 (1965)].
[10] F. W. Byron, Jr., M. N. McDermott, and R. Novick, Phys. Rev. **134**, A615 (1964).
[11] E. B. Saloman and W. Happer, Phys. Rev. **144**, 7 (1966).

average quadrupole moment is said to be "aligned," while an ensemble of atoms with a nonzero average magnetic dipole moment is called an "oriented" ensemble. It is of interest to measure both of these relaxation times since their ratio provides direct information about the importance of "soft" collisions in impact-broadening theories. Both relaxation times were measured in these experiments.

Radiation trapping has been one of the chief impediments to the study of optical-double-resonance linewidths at high atomic densities. This is particularly serious for resonance lines with large oscillator strengths. It is practically impossible to obtain undistorted line shapes under such conditions. Furthermore, radiation trapping drastically reduces the signal-to-noise ratio. It has been shown[11] that these difficulties do not occur when untrapped cross-fluorescent light is used to monitor the Hanle-effect signal. In these experiments cross-fluorescent light was used to measure Hanle-effect linewidths up to atomic densities of about 2×10^{16} atoms/cm^3.

II. THEORY

Since no clear distinction between "orientation" and "alignment" lifetimes is normally made in the literature, a brief derivation of the Breit-Franken formula for atoms in an isotropic environment will be presented in this section. Consider a vapor of identical atoms with no hyperfine structure. The resonant scattering process may be described in the following manner.[12]

(1) Some of the atoms absorb a photon. Let $\Delta\nu_D$ be the spectral width of the exciting light. It is permissible to think of the absorption as an instantaneous process since the correlation time of the exciting light beam $1/2\pi\Delta\nu_D$ is normally much shorter than the radiative lifetime or the Larmor period of the excited state.[13] Immediately after excitation each excited atom is described by a wave function $|\psi\rangle$ of the form

$$|\psi\rangle \propto \sum_m |m\rangle\langle m|\hat{e}\cdot\mathbf{p}|\psi_g\rangle. \quad (2)$$

Here $|\psi_g\rangle$ is the initial ground-state wave function of the atom, $\hat{e}$ is the polarization vector of the exciting light, and $\mathbf{p}$ is the electric dipole moment operator. The density matrix describing the ensemble of excited atoms immediately after excitation is then

$$\rho_{mm'}(0) \propto \sum_\mu \langle m|\hat{e}\cdot\mathbf{p}|\mu\rangle\langle\mu|\hat{e}^*\cdot\mathbf{p}|m'\rangle. \quad (3)$$

To obtain Eq. (3) from Eq. (2), we have assumed that the atoms are not polarized in their ground state, so that

$$(|\psi_g\rangle\langle\psi_g|)_{\rm av}=[(2J_g+1)]^{-1}\sum_\mu |\mu\rangle\langle\mu|, \quad (4)$$

where $(\ )_{\rm av}$ denotes an ensemble average over the initial ground-state wave functions. In the discussion which follows, J_g is the angular momentum of the ground state, J_e is the angular momentum of the excited state, and J_b is the angular momentum of the branch state involved in the cross fluorescence. The Zeeman sublevels of these states will be denoted by $|\mu\rangle$, $|m\rangle$, and $|n\rangle$, respectively. In operator form Eq. (3) may be written as (see the Appendix)

$$\rho(0)=-\sum_L (-1)^{J_e-J_g}3W(11J_eJ_e;LJ_g)E^L\cdot T^L. \quad (5)$$

(2) The individual excited atoms of the ensemble evolve under the influence of externally applied electromagnetic fields, radiative decay, radiation trapping, and collisions with other atoms and with the walls of the container. Following excitation the atoms are no longer affected by the exciting light. Since one assumes that the atoms are subject to random collisions, each atom of the ensemble has a different Hamiltonian, and each wave function evolves in a different way. However, it is not necessary to trace through the different histories of all of the atoms of the ensemble. Only the density matrix $\rho(t)$ enters into the theoretical expression for the fluorescent intensity. Thus, it is sufficient to obtain the Liouville operator $\mathfrak{L}$. The evolution of the density matrix is then described by the Liouville equation

$$(d/dt)\rho_{mm'}=\mathfrak{L}_{mm';m''m'''}\rho_{m''m'''}. \quad (6)$$

(3) During the course of their evolution, the excited atoms of the ensemble continuously emit light. The intensity of fluorescent light with a polarization vector $\hat{u}$ emitted by a single atom into the solid angle $d\Omega$ at a time t after excitation is[4]

$$\bar{I}(\Omega)d\Omega\propto d\Omega\sum_n \langle n|\hat{u}\cdot\mathbf{p}|\psi_e(t)\rangle\langle\psi_e(t)|\hat{u}^*\cdot\mathbf{p}|n\rangle. \quad (7)$$

It is convenient to introduce a measuring operator M which contains information about the polarization of the fluorescent light and the degree to which the light is trapped.

$$M\propto\sum_n \hat{u}\cdot\mathbf{p}|n\rangle\langle n|\hat{u}^*\cdot\mathbf{p}. \quad (8)$$

In operator form M may be written as (see Appendix)

$$M=(1-x_b)(3\Gamma_b/8\pi)(-1)^{J_b-J_e}(2J_e+1)\times\sum_L W(11J_eJ_e;LJ_b)U^L\cdot T^L. \quad (9)$$

Here $(1-x_b)$ is the probability that a fluorescent photon will escape from the vapor without being reabsorbed. The cross-fluorescent branching ratio is Γ_b/Γ, where $1/\Gamma$ is the natural radiative lifetime of the excited state. The detected light is characterized by the polarization tensors $U_M{}^L$. After averaging Eq. (7) over N excited atoms of the ensemble, one finds that the instantaneous fluorescent intensity is

$$\bar{I}(\Omega)d\Omega=N\,{\rm Tr}\{\rho(t)M\}d\Omega. \quad (10)$$

To obtain the steady-state intensity $d\bar{I}$, one must add

[12] J. P. Barrat, Proc. Roy. Soc. (London) **A263**, 371 (1961).

[13] When the coherence time becomes comparable to or greater than the Larmor period of the excited atom, the zero-field level-crossing signals are distorted. This is because the absorption profile of the scattering atoms is scanned out of the lamp profile before a complete Hanle-effect linewidth is obtained.

the instantaneous intensities of many ensembles which were excited at all initial times t_0 from $t_0=t$ to $t_0=-\infty$. If $N=z dt_0$ atoms are excited in a time interval dt_0, then

$$\bar{I}(\Omega)\,d\Omega = d\Omega \int_{-\infty}^{t} \mathrm{Tr}\{\rho(t-t_0)\,M\}\,z\,dt_0$$

$$= d\Omega\, z \int_0^{\infty} \mathrm{Tr}\{\rho(t)\,M\}\,dt. \qquad (11)$$

From Eq. (11) it is apparent that one must solve Eq. (6) for $\rho(t)$ in order to obtain an explicit expression for the fluorescent intensity. Experimental conditions are frequently approximately isotropic, so that an ensemble of polarized excited atoms relaxes in the same way regardless of the initial direction of polarization. If there are external magnetic fields (but not external electric fields), conditions are usually still isotropic in an appropriate rotating coordinate system. This greatly simplifies the Liouville equation [Eq. (6)] since it must now describe the separate exponential decay of each multipole moment of the ensemble of excited atoms (see Sec. III). Consider the case where a single static magnetic field causes a depolarization of the fluorescent light (the Hanle effect). Let σ be the density matrix in a coordinate system rotating with the Larmor frequency ω.[14] Then Eq. (6) assumes the form[15]

$$d\sigma_M{}^L/dt = -\Gamma^{(L)}\sigma_M{}^L, \qquad (12)$$

where

$$\sigma_M{}^L = \mathrm{Tr}(\sigma T_M{}^{L\dagger}). \qquad (13)$$

Equation (12) describes the exponential decay of the 2^L-pole moment of the ensemble of excited atoms. If the value of the density matrix at time $t=0$ is $\sigma_M{}^L(0)$, then the solutions of Eq. (12) specify the density matrix at all later times.

$$\sigma(t) = \sum_{LM} \sigma_M{}^L(0)\,T_M{}^L \exp(-\Gamma^{(L)}t). \qquad (14)$$

The density matrix ρ in the laboratory coordinate system is related to the density matrix σ by the transformation[14]

$$\rho(t) = \exp(-iJ_z\omega t)\,\sigma(t)\,\exp(iJ_z\omega t)$$

$$= \sum_{LM} \sigma_M{}^L(0)\,T_M{}^L \exp[-(\Gamma^{(L)}+iM\omega)t]. \qquad (15)$$

Since $\sigma(0)=\rho(0)$, one can use Eq. (5) to obtain

$$\rho(t) = (-1)^{J_g-J_e}3 \sum_{LM} W(11J_eJ_e;\,LJ_g)$$

$$\times(-1)^M E_{-M}{}^L T_M{}^L \exp[-(\Gamma^{(L)}+iM\omega)t]. \qquad (16)$$

From Eqs. (9), (11), (16), and (A2) one can now derive an explicit expression for the intensity of fluorescent light;

$$\bar{I}_b d\Omega = d\Omega\, z(1-x_b)\,(9\Gamma_b/8\pi)\,(-1)^{J_b-J_g}(2J_e+1)$$

$$\times \sum W(11J_eJ_e;\,LJ_b)\,W(11J_eJ_e;\,LJ_g)$$

$$\times \frac{(-1)^M E_{-M}{}^L U_M{}^L}{\Gamma^{(L)}+iM\omega}. \qquad (17)$$

Equation (17) is a specialization of the Breit-Franken formula[16] to the zero-field level crossings of atoms with no hyperfine structure.

It is interesting to notice that the Hanle-effect signals depend in the same way on the polarization vectors of the light, regardless of the angular momenta of the atomic states involved. The dependence of the intensity on the magnetic field is contained in the factor

$$y_L = \sum_M \frac{(-1)^M E_{-M}{}^L U_M{}^L}{1+iM\omega/\Gamma^{(L)}}. \qquad (18)$$

Only the Larmor frequency ω of the excited state and the multipole relaxation times $1/\Gamma^{(L)}$ appear in Eq. (18). Consequently, the Hanle-effect line-shape formula calculated with a purely classical model[17] is correct for any possible combination of atomic angular momenta in the initial state, excited state, and branch state. The sign and amplitude of the signal depend on the factor

$$W_L = (-1)^{J_g-J_b}(2J_e+1)\,W(11J_eJ_e;\,LJ_b)$$

$$\times W(11J_eJ_e;\,LJ_g). \qquad (19)$$

The factor W_L can be positive or negative, depending on the angular momenta of the states involved. In Table I we have evaluated W_L for the angular momenta of interest in these experiments. Equation (17) may now be written as[18]

$$\bar{I}(\Omega)\,d\Omega = d\Omega\, z(1-x_b)\,(9/8\pi) \sum_L \frac{\Gamma_b}{\Gamma^{(L)}} W_L y_L. \qquad (20)$$

At most, two different relaxation times $1/\Gamma^{(1)}$ and $1/\Gamma^{(2)}$ can be obtained from Hanle-effect experiments. If the angular momentum of the excited state is $\frac{1}{2}$, then no quadrupole moment exists and only $\Gamma^{(1)}$ can be

[14] I. I. Rabi, N. F. Ramsey, and J. Schwinger, Rev. Mod. Phys. **26**, 167 (1954).

[15] See, for instance, V. Heine, *Group Theory in Quantum Mechanics* (Pergamon Press, Inc., New York, 1960).

[16] P. A. Franken, Phys. Rev. **121**, 508 (1961).

[17] A. Lurio, R. L. deZafra, and R. Goshen, Phys. Rev. **134**, 1198 (1964).

[18] The same procedure has been used to classify the linewidths in optical-double-resonance and light-beat experiments as originating from the relaxation of alignment or orientation. Equation (20) remains the same except that the line-shape factor $y^{(L)}$ must be replaced by

$$y^{(L)} = \sum_M \frac{(-1)^M E_{-M}{}^L D_{MM'}{}^L(R)\,D_{M'M''}{}^L(R^{-1})\,U_{M''}{}^L}{\Gamma^{(L)}+i(M\omega+M'\Omega)}$$

$$\times\exp[i(M-M'')\omega t],$$

where $R=\exp(i\theta J_y)$ is a rotation operator, $\Omega=[(\omega-\omega_0)^2+\omega_1{}^2]^{1/2}$ is the nutational frequency, ω_1 measures the rf field strength, ω is the rf frequency, ω_0 is the Larmor frequency, and $\tan\theta=\omega_1/(\omega_0-\omega)$. The time-independent parts of this expression give the Brossel-Majorana formula (Ref. 1), while the time-dependent parts describe the light modulation signals first investigated by Series. [J. N. Dodd and G. W. Series, Proc. Roy. Soc. (London) **A263**, 353 (1961)]. This formula applies to the case where the rf field can be approximated by a rotating magnetic field.

TABLE I. Amplitude factors for the Hanle-effect signals studied in this experiment. [See Eq. (19) and Fig. 9.]

$$W_L=(3)(-1)^{J_g-J_b}W(1111;LJ_g)W(1111;LJ_b).$$

J_g \ J_b	W_0 0	1	2	W_1 0	1	2	W_2 0	1	2
0	$\frac{1}{3}$	$\frac{1}{3}$	$\frac{1}{3}$	$\frac{1}{3}$	$\frac{1}{6}$	$-\frac{1}{6}$	$\frac{1}{3}$	$-\frac{1}{6}$	1/30
1	$\frac{1}{3}$	$\frac{1}{3}$	$\frac{1}{3}$	$\frac{1}{6}$	1/12	−1/12	$-\frac{1}{6}$	1/12	−1/60
2	$\frac{1}{3}$	$\frac{1}{3}$	$\frac{1}{3}$	$-\frac{1}{6}$	−1/12	1/12	1/30	−1/60	1/300

observed.[19] This follows formally from the triangle relation $\Delta(J_eJ_eL)$ for the arguments of the Racah coefficients in Eq. (19).

It is convenient to label the separate terms in Eq. (18) according to the value of $|M|$ as "$\Delta M=|M|$ level crossings." Signals with $\Delta M=0$ do not depend on the magnetic field ω. However, both $\Delta M=1$ and $\Delta M=2$ level crossings give rise to easily measured field-dependent signals. The signals originating from alignment are characterized by both $\Delta M=2$ and $\Delta M=1$ level crossings, while the signals originating from orientation are characterized solely by $\Delta M=1$ level crossings.

The dominant relaxation mechanisms for excited atoms are radiative decay, radiation trapping, and collision broadening, so that it is convenient to write $\Gamma^{(L)}$ in the form

$$\Gamma^{(L)}=\Gamma-\sum_b x_b\alpha_b{}^{(L)}\Gamma_b+\gamma_L. \tag{21}$$

The radiative lifetime of the excited state is $1/\Gamma$. The second term in Eq. (21), representing the effects of radiation trapping, is discussed in detail in Ref. 11. The effects of depolarizing collisions are represented by the third term, γ_L (see Refs. 6, 8, and 9).

III. PHYSICAL MEANING OF DIFFERENT RELAXATION TIMES

An atomic state with total angular momentum J_e may have $2J_e+1$ different multipole moments. One may speak of an ensemble multipole moment which is the ensemble-averaged multipole moment of many individual atoms. The 2^L-pole moment of the ensemble is proportional to the 2^L-pole components $\rho_M{}^L$ of the density matrix. When radiation trapping and collisions are absent, all ensemble multipole moments of an excited state relax with the same lifetime, the radiative lifetime $1/\Gamma$. When radiation trapping and collisions become significant, the different ensemble multipole moments still relax exponentially,[20] but the relaxation times can be greater or less than the radiative lifetime of the state. Of course, this is a statistical phenomenon and the multipole moments of individual atoms may fluctuate wildly due to collisions.

[19] A. Gallagher and A. Lurio, Phys. Rev. Letters **10**, 515 (1963).

[20] This is only approximately true for radiation trapping. See M. I. D'yakonov and V. I. Perel', Zh. Eksperim. i Teor. Fiz. **47**, 1483 (1965) [English transl.: Soviet Phys.—JETP **20**, 997 (1965)].

The appearance of multipole relaxation times when conditions are isotropic is entirely analogous to the appearance of hyperfine energies E_F for the interaction of the electrons of a free atom with the nucleus. The Schrödinger equation for the atom,

$$(d/dt)\psi_m{}^F=-(iE_F/\hbar)\psi_m{}^F, \tag{22}$$

may be compared with the Liouville equation [Eq. (12)]. The wave functions,

$$\psi_m{}^F=\sum_\mu \psi_\mu{}^I\psi_{m-\mu}{}^J C(IJF;\mu, m-\mu),$$

play the role of the multipole components of the density matrix $\sigma_M{}^L$. The close similarity is, of course, a result of the requirement that both the Schrödinger equation and the Liouville equation describe isotropic processes.

It is instructive to consider the relationship between the multipole relaxation times and the longitudinal and transverse relaxation times τ_1 and τ_2 which are observed in many spin-resonance experiments.[21] The longitudinal and transverse relaxation times have a precise significance only for a spin-$\frac{1}{2}$ system. Here the density matrix is composed of a scalar and dipole part

$$\rho=\rho^0+\rho^1.$$

One can assume that the population of the ensemble is constant, so that ρ^0 does not relax. Under completely isotropic conditions the decay of the ensemble dipole moment is characterized by a single relaxation time $1/\gamma_1$. In this case the longitudinal and transverse relaxation times are equal. Now assume that a strong magnetic field reduces the spherical symmetry to axial symmetry. Then one can use the usual symmetry arguments[15] to show that the Liouville equation has the form

$$(d/dt)\rho_M{}^L=-\sum_{L'}\Gamma_{LL'}{}^M\rho_M{}^{L'},$$

where

$$\Gamma_{LL'}{}^{-M}=(\Gamma_{LL'}{}^M)^*.$$

One may make the identification

$$\tau_1=1/\Gamma_{11}{}^0 \quad \text{and} \quad \tau_2=1/\mathrm{Re}\Gamma_{11}{}^1.$$

Thus a longitudinal and transverse relaxation time can result from the "Zeeman splitting" of a single dipole relaxation time. Note also that since the relaxation coefficients are complex, a frequency shift can occur when an isotropic environment is replaced by an axially symmetric environment.[22]

IV. EXPERIMENTAL

A. Apparatus (Alignment)

The basic apparatus which is necessary for the observation of the Hanle effect is a source of resonance

[21] N. Bloembergen, E. M. Purcell, and R. V. Pound, Phys. Rev. **73**, 679 (1948).

[22] A. Omont, Compt. Rend. **252**, 861 (1961); E. Otten, Naturwiss. **7**, 157 (1964); A. Omont, Compt. Rend. **258**, 1193 (1964).

radiation, a magnetic field, a supply of scattering atoms, and a means of detecting the scattered light. A schematic diagram of the equipment used to observe alignment level-crossing signals is shown in Fig. 1.[23] A flow lamp was used to produce 2833-Å lead resonance light. The light was focused by fused-quartz lenses into a cylindrical fused-quartz scattering cell, 1 in. long and 1 in. in diam, which was contained in an electrically heated cell oven. The static magnetic field was produced by calibrated Helmholtz coils. Light scattered at right angles to both the incident light direction and the magnetic field was collected, passed through a 3639-Å interference filter, and was detected by a photomultiplier tube. Zeeman modulation with phase-sensitive detection was used. For small modulation amplitudes the resulting signal is the derivative of the dc Hanle-effect signal [Eq. (18)]. For the experimental arrangement described in this section, Eq. (18) reduces to

$$y \propto ((\Gamma^{(2)})^2+4\omega^2)^{-1}, \qquad (23)$$

where ω is the Larmor frequency of the excited state and $\Gamma^{(2)}$ is the total alignment relaxation rate [see Eq. (21)].

The scattering cells were prepared with great care. A two-step bake-out procedure was used to minimize foreign-gas contamination. First, the cell and most of the vacuum system were baked out under vacuum at 250°C for about 24 h. Then the cell and the distillation portion of the vacuum system were baked out for another 24 h under a vacuum of 10^{-6} Torr at a temperature which was at least 100°C above the highest temperatures to be used in the experiments, temperatures as high as 1150°C being attained. After bake-out, the cell was filled with a few milligrams of 99.75% isotopically pure Pb^{208} (nuclear spin zero). The use of a separated isotope eliminates any confusion with the Hanle-effect signal from the odd isotope Pb^{207} (nuclear spin $\frac{1}{2}$).

The cell heating oven was constructed of nickel and was always operated above the Curie temperature. The cell was situated in the oven in such a way that all of the region containing excited atoms was "seen" by the photomultiplier. No significant change in the detection solid angle [Eq. (17)] occurred as the density of the scattering atoms increased since the cross-fluorescent light was not trapped and since all visible regions of the vapor subtended practically the same solid angle at the photomultiplier tube. The cell oven was surrounded with a silver radiation shield in order to decrease thermal gradients across the oven. In addition, slotted oven windows were used to reduce radiation losses through the windows. In spite of these precautions, thermal gradients across the cell as high as 30°C were measured at the highest temperatures attained (1050°C). Atomic densities were calculated by using the ideal gas law and vapor-pressure–versus–temperature data.[24] In these experiments the temperatures were measured at a fixed point on the absorption cell. A separate set of measurements related the temperature of this fixed point to that at the coolest part of the cell. The temperature used in the density computations was the estimated temperature at the coolest part of the cell.

[23] A detailed description of this apparatus can be found in Ref. 11.

B. Data Taking

The width of the observed Hanle-effect signal was studied as a function of Zeeman modulation amplitude. Afterward, a very small modulation, corresponding to about a 1% broadening of the signal, was used, and the signal width was corrected for this small broadening. Sweep rates and lock-in integration time constants were chosen so that the corrections to the signal width needed to account for the finite integration time were negligible.

In spite of all precautions, there was a tendency for the scattering cells to become gassy. The foreign gas resulted in a small broadening of the signal width. The amount of this broadening was determined by observing the signal width in the density region around 10^{13} atoms/cm^3 where saturated coherence narrowing occurs but where self-broadening is not important (see Fig. 2). The gas broadening is the difference between this width and the corresponding width in a gas-free cell. Since the walls of the quartz cell evolved foreign gas continuously, especially at temperatures above 900°C, frequent checks of the gas broadening were made, and any foreign-gas broadening was subtracted from the measured widths. The foreign-gas broadening should not depend strongly on temperature, so that the same correction was made at all temperatures. After this correction the results obtained from gassy cells agreed with those from gas-free cells to well within the statistical uncertainty in the data.

C. Apparatus (Orientation)

A slight modification of the apparatus made it possible also to observe orientation relaxation times (Fig. 3). The rationale for this apparatus was the following:

(1) *Polarization analyzer for the detected light (Fig. 4).* The polarization vectors of the light accepted by the analyzer were $(u_1, u_0, u_{-1}) = (-\sin\alpha, \cos\alpha, 0)$ with $\tan\psi = \frac{1}{2}\sqrt{2}\tan\alpha$. The corresponding components of the polarization tensor were $U_{\pm 2}{}^2 = 0$, so that no $\Delta m = 2$ signal could be detected [see Eq. (18)], but $U_1{}^2 = U_1{}^1 = (\sin 2\alpha)/2\sqrt{2}$ (see Appendix). Thus, the elliptical analyzer acted as a discriminator for $\Delta M = 2$ signals. The tensor components $U_1{}^2$ and $U_1{}^1$ attain their maximum value for $\alpha = \pi/4$ which corresponds to $\psi = 35°$ (see Fig. 4). It was not possible to place the detection light pipe at this angle because the Helmholtz coils were in the way. Instead, an angle $\psi = 45°$ was chosen which still gave fairly large $\Delta M = 1$ signals.

[24] R. Hultgren, R. L. Orr, P. D. Anderson, and K. K. Kelley, *Selected Values of Thermodynamic Properties of Metals and Alloys* (John Wiley & Sons, Inc., New York, 1963), pp. 206 ff.

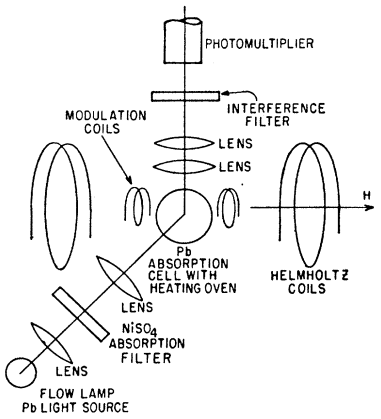

FIG. 1. Apparatus used to measure alignment relaxation times.

(2) *Polarizer for the exciting light.* Since the elliptical analyzer rejects $\Delta M=2$ signals but accepts $\Delta M=1$ signals from both orientation and alignment, a signal width characterized solely by $\Gamma^{(1)}$ will result if the polarization tensors of the exciting light are such that $E_1^2=0$ but $E_1^1\neq 0$. One can easily show that if the incident light in Fig. 3 is circularly polarized, then $(e_1, e_0, e_{-1})=(-\frac{1}{2}, i/\sqrt{2}, +\frac{1}{2})$ and $E_1^2=0$ while $E_1^1=-i/2$. Using Eq. (18) one finds that the signal has the form

$$y\propto \omega/((\Gamma^{(1)})^2+\omega^2). \tag{24}$$

This signal is a pure dispersion curve characterized by the orientation width $\Gamma^{(1)}$. Analogous arguments show that if the incident light in Fig. 3 is linearly polarized

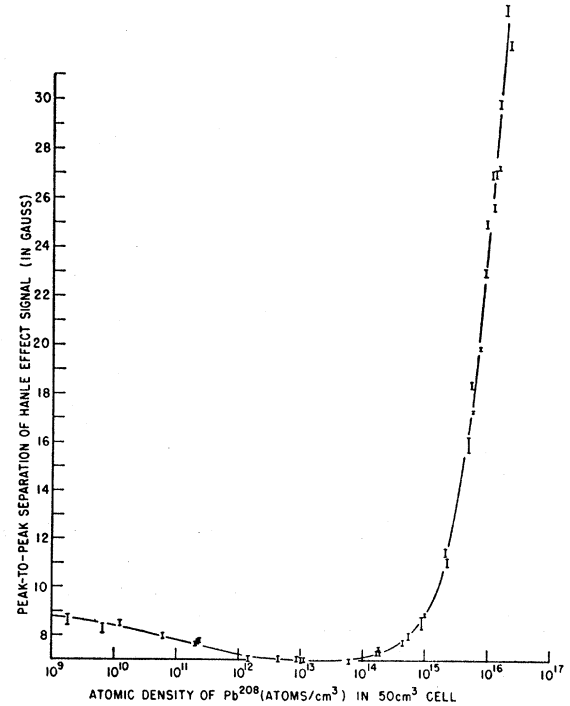

FIG. 2. Alignment linewidth versus atomic density.

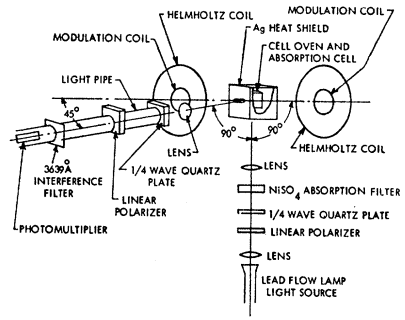

FIG. 3. Apparatus used to measure orientation relaxation times.

at a 45° angle to the magnetic field direction, then the resulting signal will have the form

$$y\propto 1/((\Gamma^{(2)})^2+\omega^2). \tag{25}$$

This signal is a pure Lorentzian curve characterized by the alignment relaxation time $\Gamma^{(2)}$.

Since the ellipticity of the analyzer was quite critical in these experiments, mica quarter-wave plates proved to be very unsatisfactory. Even the most carefully prepared mica sheets were found to have relative phase shifts a few degrees greater or less than 90°. A very convenient, tunable quarter-wave plate was finally used (Fig. 5). By stressing a plate of fused quartz any relative retardation from 0° to well over 180° can be obtained.[25] However, these phase plates were very sensitive to temperature changes. Temperature-regulated water was circulated around the analyzer to minimize thermal drift, and ample time was allowed for the apparatus to come to thermal equilibrium before any data were taken. Nevertheless, some residual drift remained, and at regular intervals throughout the course of these measurements it was necessary to check to see if any drift of the phase-shift plates had occurred.

The polarizers were adjusted in the following way. The polarizer in the incident arm was removed and the ellipticity of the analyzer was adjusted until no signal was recorded upon sweeping the magnetic field through zero. Since $E_{\pm 2}^2$ (and, of course, E_0^0) are the only non-

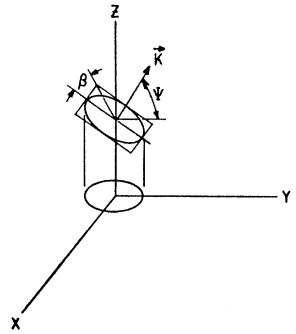

FIG. 4. The elliptical polarization accepted by the analyzer. The projection of the ellipse onto the plane which is perpendicular to the static magnetic field is a circle. Consequently, $\tan\beta=\sin\psi$. An auxiliary angle α, which is mentioned in the text, is not shown.

[25] These phase-shift plates were kindly lent to us by A. Lurio, R. Garwin, and A. Patlach of IBM Watson Laboratory, Columbia University, New York.

zero components of the exciting light polarization tensor, the absence of a signal implied that the $\Delta M=2$ level-crossing signal had been completely rejected [i.e., that $U_{\pm 2}{}^2=0$; see Eq. (18)]. Then the circular polarizer was inserted in the input arm and adjusted until a symmetric signal was obtained upon sweeping through zero magnetic field. [Since Zeeman modulation and phase-sensitive detection were used, the observed signal was approximately the derivative of Eq. (24).] Typical results of this adjustment procedure are shown in Fig. 6. At least six orientation curves were obtained at each of several modulation amplitudes, and the effective width at zero modulation amplitude was obtained by extrapolation.

Alignment widths were measured using $\Delta M=2$ level crossings as described in Sec. IVA, and they were also measured using $\Delta M=1$ crossings. The experimental procedure was the same as that described for the orientation linewidth measurements except that the incident light was linearly polarized. [See the discussion of Eq. (25).] The alignment relaxation rates $\Gamma^{(2)}$ measured by both methods agreed to within the statistical uncertainty of the data. Since the beam angles and polarizers were quite different for these two methods, the agreement indicates that any systematic error due to misalignment of the optical equipment was insignificant.

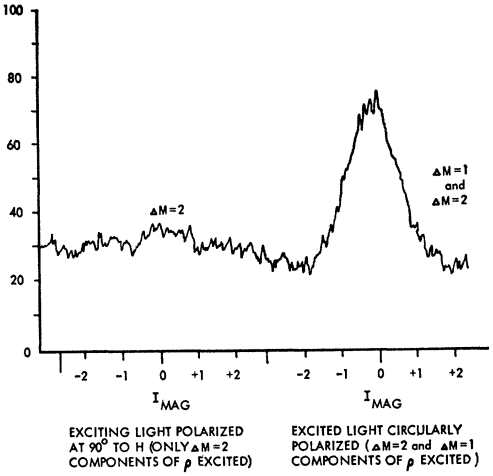

FIG. 6. Rejection of the $\Delta M=2$ signal by the elliptical analyzer.

V. DISCUSSION OF RESULTS

A. Alignment Collision-Broadening Cross Section

The results of all alignment linewidth measurements are plotted in Fig. 2. Three fairly distinct density regions can be delineated.

(1) $N \lesssim 10^{10}$ atoms/cm^3: For these low densities an excited atom is essentially free during its lifetime. The true radiative lifetime of the atom may be deduced from the limiting value of the linewidth in this low-density region.

(2) 10^{10} atoms/cm$^3 \lesssim N \lesssim 10^{14}$ atoms/cm^3: In this region, radiation trapping causes a narrowing of the linewidth. This effect occurs when the interatomic interactions are due chiefly to the first term in Eq. (1).

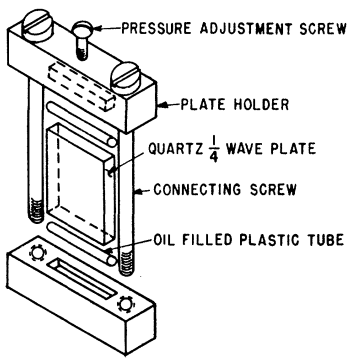

FIG. 5. The adjustable quartz phase-shift plate (see Ref. 25).

The effect on the linewidth is described by the second term in Eq. (21). At high densities this term approaches the saturation value $\alpha^{(2)}(\Gamma_0/\Gamma)\,\Gamma=(7/10)\,(0.27)\,\Gamma$ since only the 2833-Å light is appreciably trapped.[11]

(3) 10^{14} atoms/cm$^3 \lesssim N \lesssim 10^{16}$ atoms/cm^3: In this region, the rapid increase in the linewidth can be ascribed to binary-collision broadening. The dominant interaction during most binary encounters is described by the last term in Eq. (1), and the corresponding effect on the linewidth is represented by the broadening term γ_2 in Eq. (21).

The experimentally measured broadening γ_2 has been plotted versus the atomic density in Fig. 7. The broadening is proportional to the density up to about 10^{16} atoms/cm^3. One can define a broadening cross section $\sigma_2(v)$ such that

$$\gamma_2=\int N(v)\,v\sigma_2(v)\,dv, \tag{26}$$

where $N(v)dv$ is the density of colliding atoms with relative velocities between v and $v+dv$. For purely resonant collision broadening $v\sigma(v)$ is a constant[6,8,9] so that

$$\gamma_2=\bar{v}\sigma_2(\bar{v})N, \tag{27}$$

where N is the total atomic density and $\bar{v}$ is any convenient average velocity of the colliding atoms. Consequently, from Eq. (27) and from the slope of the broadening curve in Fig. 7, one can deduce that $\bar{v}\sigma_2(\bar{v})=3.8\times 10^{-8}$ cm^3/sec.

In Fig. 8 the self-broadening cross section for Pb measured in the present work is compared with several theoretical estimates and with the experimental self-broadening cross sections of Zn and Cd quoted by other authors.[10,26] All of these atoms have an excited state with atomic spin $J=1$, and the cross sections for each element were measured for an isotope without

[26] M. Dumont, thesis, Paris, 1962 (unpublished).

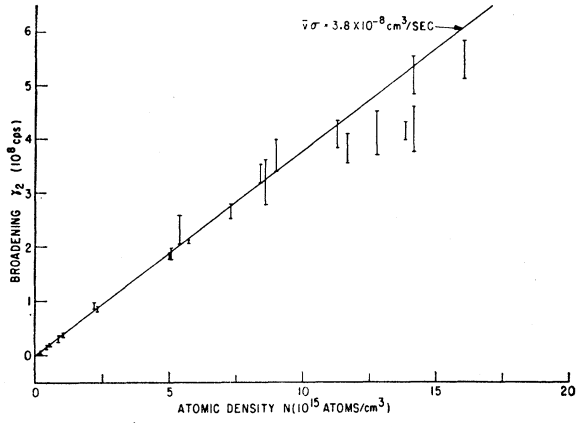

FIG. 7. Alignment broadening versus density.

hyperfine structure. As was first pointed out by Byron and Foley,[6] the experimental self-broadening cross sections for elements with small resonance line oscillator strengths are considerably larger than a first-order resonance broadening theory would predict. Higher-order contributions from the terms in Eq. (1) must be considered in order to account for such large depolarization cross sections. However, the resonance line in lead has a rather large oscillator strength[11] ($f=0.17$), and the self-broadening cross section measured in this work is in good agreement with that expected for pure resonant broadening. This cross section $\sigma\approx10^{-12}$ cm^2 is almost a thousand times larger than typical gas kinetic cross sections.

B. Orientation Collision-Broadening Cross Sections

The measurements of the orientation collision-broadening cross sections were extremely tedious because of the extensive checks that were undertaken to discover any unsuspected sources of systematic error. Consequently, orientation linewidth measurements were made for one atomic density in the collision-broadening region and for one atomic density in the coherence-narrowing region. Also orientation and alignment linewidths were measured for a gassy cell in the coherence-narrowing region. The results of these measurements are listed in Table II. A preliminary report of these measurements was given in Ref. 27. Two minor corrections have been made to the data in that paper. The temperature readings for the data in the collision-broadening region were in error because the thermocouple was not located at the coolest part of the cell. Also, in Ref. 27 the broadening γ_L was computed by subtracting from the measured width $\Gamma^{(L)}$ the natural width Γ rather than the coherence-narrowed width $\Gamma[1-\alpha_0{}^{(L)}(\Gamma_0/\Gamma)]=\Gamma_{CN}{}^{(L)}$.

The measured ratio $\gamma_1/\gamma_2=1.21(5)$ is in good agreement with the value $\gamma_1/\gamma_2=1.25(5)$ calculated by D'yakonov and Perel'[9] on the basis of a numerical solution of the collision-broadening problem using an impact theory with straight-line trajectories. It is also in fairly good agreement with the value $\gamma_1/\gamma_2=1.30\leftrightarrow1.67$ computed by Omont, who used approximate methods to perform the ensemble average over impact parameters. In the work of Byron and Foley[6] no distinction was made between alignment and orientation. It is interesting to notice that although the alignment resonance-broadening cross sections calculated in these three papers are very nearly the same, only the theory of D'yakonov and Perel' gives a ratio γ_1/γ_2 which is in good agreement with our experimental value. This is particularly significant, since any error in the determination of the atomic density cannot affect the ratio γ_1/γ_2, but it can affect the absolute cross section.

The orientation and alignment linewidths were also measured in a gassy cell. The foreign-gas broadening ratio $\gamma_1/\gamma_2=1.27$ was surprisingly large. Unfortunately, the composition and pressure of the foreign gas were not known, but a spectrographic analysis of the light from a microwave discharge in the cell showed N_2, OH, CO, and NH emission bands as well as strong lines from atomic hydrogen. It may be that collision broadening by foreign-gas molecules with permanent electric dipole moments, such as H_2O, gives rise to an unusually pronounced difference between the orientation and alignment cross sections.

VI. COMPLICATING EFFECTS AT HIGH DENSITIES

A. Thermal Population of the Metastable States

As mentioned earlier, branching in the decay of the $(6p7s)^3P_1{}^\circ$ state of lead allows one to study the relaxation of these atoms at high densities, even when the

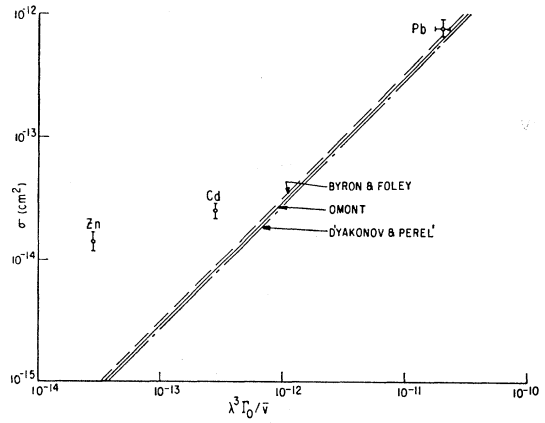

FIG. 8. Self-broadening in lead compared to theoretical predictions of resonance broadening (see Refs. 6, 8, and 9). A relative velocity of 5×10^4 cm/sec was used. Data for zinc and cadmium were taken from Refs. 10 and 26. The nonresonant broadening mechanisms which play a dominant role for zinc and cadmium are of minor importance for lead because of the large oscillator strength of the 2833-Å resonance transition.

[27] W. Happer and E. B. Saloman, Phys. Rev. Letters **15**, 515 (1965).

TABLE II. Summary of orientation and alignment relaxation rates for lead. (See Secs. V A and V B.)

Lead atomic density (atoms/cm^3)	$\Gamma^{(1)}/\Gamma$	$\Gamma^{(2)}/\Gamma$	Quantity	Experimental	Theoretical	Effect
2.4×10^{15}	1.99(3)	1.76(3)	$(\Gamma^{(1)}-\Gamma_{CN}{}^{(1)})/(\Gamma^{(2)}-\Gamma_{CN}{}^{(2)})$	1.21(5)	1.25(4)	Resonant self-broadening
1.2×10^{13}	1.36(2)	1.22(2)	$(\Gamma^{(1)}-\Gamma_{CN}{}^{(1)})/(\Gamma^{(2)}-\Gamma_{CN}{}^{(2)})$	1.27(18)	...	Foreign-gas broadening
1.2×10^{13}	0.852(18)	0.818(18)	$(\Gamma^{(1)}-\Gamma)/(\Gamma^{(2)}-\Gamma)$	0.8(2)	0.714	Saturated coherence narrowing

resonance line is heavily trapped. At very high temperatures (1000°C and above) the branch lines are also trapped. The relative population of the metastable branch states with respect to the ground state is given by the Boltzmann factor

$$\frac{N_b}{N_g}=\frac{2J_b+1}{2J_g+1}\exp\left[-\left(\frac{E_b-E_g}{kT}\right)\right], \qquad (28)$$

where E_b and E_g are the energies, and N_b and N_g are the densities of atoms in the branch state and ground state, respectively. This ratio remains small for the temperatures used in this work. However, the absolute population of the branch states can become large enough to cause significant trapping of the 3639-Å and 4058-Å cross-fluorescent light. Table III shows the absolute density of lead atoms in the three lowest states as a function of temperature.[24] The lead vapor begins to become optically thick to the 3639-Å and 4058-Å cross-fluorescent light as the temperature is increased above 1000°C (see the values of the extinction coefficients κ in Table III), and the level-crossing signals observed with cross-fluorescent light rapidly diminish in intensity. This places an upper limit on the temperature (density) at which the Hanle-effect signal can be investigated.

Most collision-broadening data were taken using the scheme shown in Fig. 9(a), since this combination of wavelengths for the exciting and detected light usually gave the largest signal-to-noise ratios. A $NiSO_4$ liquid absorption filter was used in the incident arm. It permitted 2833-Å light to pass into the resonance cell while completely absorbing 3639-Å and 4058-Å light. An interference filter in the detection arm allowed only the 3639-Å light to reach the photomultiplier tube. The dc signal in this case had a maximum at zero magnetic field, as indicated in Fig. 9(a). To confirm that the metastable levels were becoming significantly populated, we used the arrangement shown in Fig. 9(b). In the incident arm a Pyrex plate was used to absorb the 2833-Å ultraviolet line and a Schott UG-11 filter was used to absorb the visible 4058-Å line. Thus only 3639-Å light entered the resonance cell. As before, 3639-Å light was detected. At temperatures of 700°C or below no signal was observed. This indicated that there was no significant population in the $(6p)^2\ ^3P_1$ state. However, when the temperature of the resonance cell was raised to 1020°C, a signal was observed which corresponded to the dc signal sketched in Fig. 9(b). This signal had a minimum at zero magnetic field. The reversal of the dc signal is expected, as can be seen from Table I. The sign factor W_2 (see Sec. II) is $-\frac{1}{6}$ for case *a* but $\frac{1}{12}$ for case *b*. The predicted signals corresponding to the schemes indicated in Figs. 9(c) and 9(d) were also observed experimentally. The signal widths at a fixed temperature were carefully measured for all of these schemes, and they were found to be equal to within the statistical error of the measurements. This, too, is in agreement with theory [see Eqs. (17) and (21)].

B. Multiple Collisions

At high densities it becomes increasingly probable that an atom will undergo multiple collisions as well as binary collisions. The near-field terms in Eq. (1) begin to dominate over the radiation-field terms at an interactomic separation of $\lambda\!\!\!^{-}=\lambda/2\pi$. Consider a sphere of radius $\lambda\!\!\!^{-}$ and volume $\Delta V=\frac{4}{3}\pi\lambda\!\!\!^{-3}$ surrounding a given atom in the vapor. Then the probability $P(n)$ that n additional atoms lie within ΔV is a measure of the relative importance of binary ($n=1$) and multiple

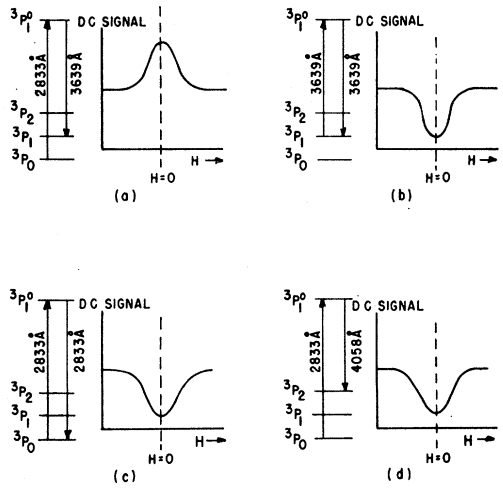

FIG. 9. Hanle-effect signals observed for various combinations of exciting light and detected light. The signals in scheme (b) were only observed at temperatures of 1000°C or greater, showing that a significant population of metastable atoms was present at these high temperatures.

TABLE III. Characteristics of lead vapor at various temperatures. Vapor-pressure data were taken from Ref. 24. The populations of the metastable states were calculated from Eq. (28). Absorption coefficients and Doppler widths were calculated from Eqs. (30), (31), and the data of Ref. 11. The mean free path of an aligned atom was estimated from the collision-broadening data of this paper. The multiple-collision probabilities were calculated from Eq. (29).

Temperature T (°C)	Atomic densities N_0 ($^3P_0$) atoms/cm^3	N_1 ($^3P_1$) atoms/cm^3	N_2 ($^3P_2$) atoms/cm^3	Absorption lengths κ_0^{-1} (cm) 2833 Å	3639 Å	4058 Å	rms velocity $\bar{v}$ (10^4 cm/sec)	Mean free path $\bar{v}\tau_2$ (10^{-4} cm)	Doppler width $\Delta\nu_0$(2833 Å) (10^9 Hz)	Multiple collision probabilities $P(0)$	$P(1)$	$P(2)$	$P(3)$
400	3.1×10^{9}	4.2×10^{2}	...	1.0×10^{2}	2.5×10^{9}	...	2.32	...	1.36	1.00	0.00	0.00	0.00
450	2.4×10^{10}	1.7×10^{4}	9.0×10^{1}	1.4×10^{1}	6.5×10^{7}	2.8×10^{9}	2.40	...	1.41	1.00	...	...	...
500	1.6×10^{11}	3.2×10^{5}	2.1×10^{3}	2.2×10^{0}	3.6×10^{6}	1.3×10^{8}	2.48	...	1.46	1.00	...	...	...
550	9.8×10^{11}	3.5×10^{6}	4.0×10^{4}	3.6×10^{-1}	3.4×10^{5}	6.8×10^{6}	2.57	...	1.50	1.00	...	...	...
600	5.3×10^{12}	4.0×10^{7}	5.7×10^{5}	6.9×10^{-2}	3.0×10^{4}	4.9×10^{5}	2.64	...	1.55	1.00	0.00	...	...
650	1.9×10^{13}	3.0×10^{8}	5.0×10^{6}	2.0×10^{-2}	4.2×10^{3}	5.8×10^{4}	2.72	...	1.60	0.99	0.01	...	...
700	6.4×10^{13}	1.95×10^{9}	4.7×10^{7}	6.0×10^{-3}	6.6×10^{2}	6.3×10^{3}	2.79	1.6	1.64	0.97	0.03	...	...
750	1.9×10^{14}	9.0×10^{9}	6.0×10^{8}	2.0×10^{-3}	1.5×10^{2}	5.1×10^{2}	2.86	1.6	1.68	0.93	0.07	0.00	...
800	5.0×10^{14}	4.1×10^{10}	1.6×10^{9}	7.9×10^{-4}	4.1×10^{1}	1.9×10^{2}	2.93	1.5	1.72	0.82	0.16	0.02	0.00
850	1.15×10^{15}	1.5×10^{11}	6.8×10^{9}	3.6×10^{-4}	9.2×10^{0}	4.7×10^{1}	3.00	1.4	1.76	0.64	0.28	0.06	0.01
900	2.5×10^{15}	5.0×10^{11}	2.7×10^{10}	1.7×10^{-4}	2.8×10^{0}	1.2×10^{1}	3.06	1.1	1.80	0.38	0.37	0.19	0.06
950	5.4×10^{15}	1.7×10^{12}	1.0×10^{11}	8.0×10^{-5}	8.5×10^{-1}	3.4×10^{0}	3.13	0.8	1.84	0.13	0.26	0.27	0.19
1000	1.05×10^{16}	4.2×10^{12}	3.1×10^{11}	4.2×10^{-5}	3.5×10^{-1}	1.1×10^{0}	3.19	0.7	1.87	0.02	0.07	0.14	0.21
1050	2.0×10^{16}	1.08×10^{13}	9.8×10^{11}	2.2×10^{-5}	1.4×10^{-1}	3.5×10^{-1}	3.25	0.4	1.91	0.00	0.00	0.01	0.03
1100	3.5×10^{16}	3.0×10^{13}	2.6×10^{12}	1.3×10^{-5}	5.1×10^{-2}	6.7×10^{-2}	3.32	0.2	1.95	0.00	0.00	0.00	0.00

($n>1$) collisions. From Poisson statistics one can show that

$$P(n)=[(\Delta VN)^n/n!]e^{-\Delta VN}. \tag{29}$$

Values of $P(n)$ are listed in Table III for small values of n. Notice that a density of 10^{16} atoms/cm^3 multiple collisions are already more likely than binary collisions, since the probablity $P(1)$ that a given atom will have a single near neighbor is already much smaller than the probability $P(2)$ that it will have two or even three near neighbors. Consequently, qualitatively new effects may occur at densities above 10^{16} atoms/cm^3. The depolarization collision-broadening theories which are available at present were developed for binary collisions with straight-line trajectories. Further theoretical work on collision broadening at high densities is clearly desirable. It is possible that an impact-broadening theory can still give satisfactory results by including the effects of the other atoms in the neighborhood during a collision in an effective dielectric constant which would shield the interacting atoms. This is the approach which was used by Barrat in his treatment of coherence narrowing.[5]

C. Specular Reflection

At extremely high atomic densities the absorption length $1/\kappa_0$ for resonance light becomes comparable to the wavelength of the light, and specular reflection will occur at the interface between the container walls and the vapor.[28] The extinction coefficient at the center of a Doppler-broadened absorption line is given by[29]

$$\kappa_0=(2/\Delta\nu_D)[(\ln 2)/\pi]^{1/2}(\pi e^2/mc)\,fN, \tag{30}$$

where the Doppler width is

$$\nu_D=2\nu_0[(2\ln 2)RT/Mc^2]^{1/2}. \tag{31}$$

Values for $1/\kappa_0$ are listed in Table III for 2833-Å, 3639-Å, and 4058-Å lead resonant light. At a density of 10^{16} atoms/cm^3 $1/\kappa_0\approx5000$ Å, somewhat greater than the wavelength of the 2833-Å exciting light, so that very little specular reflection occurred in the density range investigated in these experiments. The onset of appreciable specular reflection would considerably complicate the interpretation of the data. One could no longer think of individual atoms, excited independently by the radiation field and reradiating spontaneously without spatial coherence, as was done in Sec. II.

D. Wall Effects

Except for extremely long-lived excited states, collisions of optically excited atoms with the walls of the container can usually be neglected because the average distance $\bar{v}\tau_2$ traversed by a polarized excited atom is

[28] R. W. Wood, *Physical Optics* (Macmillan Company, New York, 1934), 3rd ed., p. 534.

[29] A. Mitchell and M. Zemansky, *Resonance Radiation and Excited Atoms* (Cambridge University Press, London, 1961).

much less than the dimensions of the container (τ_2 is the alignment relaxation time). However, most of the atoms are excited within a few optical depths of the wall of the container, and at very high densities an appreciable number of atoms can be excited within $\bar{v}\tau_2$ of the container walls. An excited atom which strikes the walls before completing the process of emission will very likely be completely disoriented, and it may also be quenched by nonradiative deactivation against the cell wall. Wall collisions may have two effects:

(1) Because of the premature interruption of the radiation process, the level-crossing linewidth may be broadened. This broadening must be distinguished from the true self-broadening.

(2) The statistical environment of an ensemble of atoms very close to the cell walls is no longer isotropic. Consequently, the characterization of the density matrix by multipole moments which relax independently is not necessarily correct.

Wall effects are certainly negligible at atomic densities below about 3×10^{15} atoms/cm^3 since $1/\kappa_0$ is greater than $\bar{v}\tau_2$ up to this density (see Table III). Actually, $1/\kappa_0$ is an underestimate of the average distance of the excited atoms from the walls since it only measures the attenuation at the center of the absorption profile, and any optical collision broadening is neglected in Eq. (30). We have also worked out a simple model of this type of wall broadening by assuming that the number of excited atoms decreases exponentially as one moves away from the wall and that the velocity distribution of excited atoms is monochromatic but isotropic. The surprising result is that the wall broadening is zero in both the low-density limit (wall collisions negligible) and the high-density limit (half of the atoms hit the walls). The maximum broadening, which occurs at some intermediate density, does not exceed 25%. The reason for this behavior is that excited atoms moving away from the walls are not affected at all, while atoms which have their lifetimes appreciably shortened by wall collisions emit much less light and thus contribute very little to the average line shape.

E. Diatomic Molecules

The molecule Pb_2 is known to exist.[30] Recent experimental work[31] has demonstrated that no significant concentration of Pb_2 occurs in the density range investigated in this work.

VII. CONCLUSIONS

The large self-broadening cross sections measured in this work support the assumption that the collision-broadening mechanism in the $(6s^2 6p7s)$ state of lead involves resonant transfer of excitation during binary encounters. We have shown that both orientation and alignment cross sections can be measured in Hanle-effect experiments. Under certain circumstances, optical-double-resonance and light-beat experiments would allow a more convenient separation of orientation and alignment signals since less stringent requirements on the circular polarizers are necessary. This is because an extra degree of freedom is present in the frequency of the detected signal. The measurement of the ratio of orientation and alignment cross sections can provide a more stringent test of collision-broadening theories than absolute alignment cross-section measurements. In particular, this ratio is sensitive to the number of soft collisions in impact-broadening theories since hard (completely disorienting) collisions result in equal orientation and alignment relaxation times. An extension of these studies to foreign-gas broadening by gases with permanent electric moments would be of interest since the long-range interactions between the quadrupole moment of the excited atom and the electric fields of the perturbing molecule could result in large differences between orientation and alignment relaxation times. Further studies of polarization phenomena in high-density vapors would also be extremely interesting since here many of the basic approximations used to analyze level-crossing experiments are no longer valid.

ACKNOWLEDGMENTS

The authors would like to express their gratitude to Professor R. Novick for his interest and encouragement during the course of this work. It is a pleasure to acknowledge the help of A. Baratta in the experimental phase of the work.

APPENDIX

Since the appearance of separate lifetimes for orientation and alignment stems from the isotropic physical environment of the excited atoms (see Sec. III), it is convenient to use a mathematical formalism which is adapted to the existing literature on the coupling of angular momenta. Operators within the excited-state subspace will be expressed in terms of the irreducible tensors[32,33] $T_M{}^L$. By definition

$$T_M{}^L=\sum |\, Jm\rangle\langle J,\, m-M \,|\, (-1)^{m-M-J} \times C(JJL;\, m,\, M-m). \quad \text{(A1)}$$

The tensors $T_M{}^L$ form a complete orthonormal set since

$$\mathrm{Tr}\{T_M{}^L T_{M'}{}^{L'\dagger}\}=\delta_{LL'}\delta_{MM'}. \quad \text{(A2)}$$

[30] M. Domaniewska-Krüger, Acta Phys. Polon. **1**, 357 (1932).
[31] J. H. Kim and A. Cosgarea, Jr., J. Chem. Phys. **44**, 806 (1966).
[32] U. Fano, Rev. Mod. Phys. **29**, 74 (1957).
[33] The notation used is that of M. E. Rose, *Elementary Theory of Angular Momentum* (John Wiley & Sons, Inc., New York, 1957).

From Eq. (A1) one can show that

$$T_M{}^{L\dagger}=(-1)^M T_{-M}{}^L. \tag{A3}$$

It is useful to define polarization tensors $E_M{}^L$ for a light beam with the polarization vector $\hat{e}$.

$$E_M{}^L=\sum_\mu e_\mu (e_{\mu-M})^*(-1)^{\mu-M-1}C(11L;\,\mu,\,M-\mu). \tag{A4}$$

From Eq. (A4) one can show that

$$E_M{}^1=(i/\sqrt{2})[\hat{e}^*\times\hat{e}]_M, \tag{A5}$$

so that $E_M{}^1$ is identically zero for linearly polarized light.

Consider a triad of mutually perpendicular vectors ${}^1\hat{e}$, ${}^2\hat{e}$, and ${}^3\hat{e}$. A useful identity relates the components of the corresponding polarization tensors:

$${}^1E_M{}^L+{}^2E_M{}^L+{}^3E_M{}^L=\sqrt{3}\delta_{L,0}\delta_{M,0}. \tag{A6}$$

This may be proved by verifying Eq. (A6) for the special case of unit vectors ${}^i\hat{e}$ along the x, y, and z axes of a Cartesian coordinate system. Since any other triad of unit vectors can be obtained from the special case by a rotation, Eq. (A6) is also true in general since it is a tensor equation.

Consider a solid angle $d\Omega$ around the direction ${}^3\hat{e}$. Choose two other unit vectors ${}^1\hat{e}$ and ${}^2\hat{e}$, so that ${}^1\hat{e}$, ${}^2\hat{e}$, and ${}^3\hat{e}$ are mutually perpendicular. Let ${}^\lambda E_M{}^L$ be the polarization tensor corresponding to ${}^\lambda\hat{e}$. Then

$$\sum_{\lambda=1,2}\int_{4\pi}{}^\lambda E_M{}^L d\Omega=\frac{8\pi}{\sqrt{3}}\,\delta_{L,0}\delta_{M,0}. \tag{A7}$$

This follows from Eq. (A6) and from the fact that ${}^3E_M{}^L(\Omega)\propto Y_M{}^L(\Omega)$. The average value of any spherical harmonic $Y_M{}^L(\Omega)$ is zero (except for $Y_0{}^0$).

Finally, a frequently occurring scalar operator x, which operates in the Zeeman subspace $|\,Jm\,\rangle$, can be expressed in terms of irreducible tensors.

$$\begin{aligned}x&=\sum_{\mu=-I}^{+I}\hat{e}\cdot\mathbf{D}\,|\,I\mu\,\rangle\langle I\mu\,|\,\hat{e}^*\cdot\mathbf{D}\\&=-\langle J\,||\,D\,||\,I\,\rangle\langle I\,||\,D\,||\,J\,\rangle\sum_{LM}(-1)^M E_{-M}{}^L\\&\quad\times T_M{}^L W(11JJ;\,LI)[(2I+1)(2J+1)]^{1/2}.\end{aligned} \tag{A8}$$

Here $\mathbf{D}$ is any vector operator. Equation (A8) may be proved in a straightforward way from (A1), (A4), and the standard sum rules for vector-coupling coefficients.[33]

We may now easily derive the important formulas in Sec. II. Equation (5) is obtained from Eq. (3) by using Eq. (A8). The normalization of Eq. (5) is chosen such that $\mathrm{Tr}\rho(0)=1$. Equation (9) follows from Eq. (8) in a similar way. The measuring matrix M [Eq. (9)] is normalized in such a way that the total number of photons emitted into all the cross-fluorescent modes b is just equal to the excitation rate z; i.e.,

$$\sum_{b,\lambda}\int{}^\lambda I_b(\Omega)\,d\Omega=z. \tag{A9}$$

This is easily verified using Eqs. (17) and (A7). In Eq. (A9) we have added the intensities of two mutually perpendicular polarization modes which are labeled by λ.

Finally, we should point out that an unpolarized beam of light will produce a Hanle-effect signal equal in magnitude but opposite in sign to that which would have been produced by light, linearly polarized along the direction of propagation of the beam. This is obvious physically since if one more polarization component were added to the beam, the exciting light would be isotropic and no Hanle-effect signal would be observed. Thus the signal from the unpolarized beam must be just enough to cancel out the signal from a third component of polarization if it were there. The same conclusion follows formally from the identity (A6).